

# ASSESSMENT OF THE MECHANICAL PROPERTIES OF ULTRA-HIGH PURITY NIOBIUM AFTER COLD WORK AND HEAT TREATMENT WITH THE HL-LHC CRAB CAVITIES AS BENCHMARK\*

A. Gallifa Terricabras<sup>†</sup>, A. Amorim Carvalho, I. Aviles Santillana, S. Barrière, R. Calaga, E. Cano-Pleite, O. Capatina, M.D. Crouvizier, L. Dassa, M.S. Meyer, N. Valverde Alonso, CERN, Geneva, Switzerland

M. Benke, A. Hlavács, G.J. Krallics, V. Mertinger, A.B. Palotas, M. Sepsí, G. Szabó, M. Szűcs, Faculty of Materials Science and Engineering, University of Miskolc, Miskolc, Hungary

## Abstract

The High Luminosity Large Hadron Collider (HL-LHC) is the upgrade of the world's largest particle collider; it will allow the full exploitation of the LHC potential and its operation beyond 2025. An essential part of the HL-LHC project are the Crab Cavities, that are particle deflecting SRF cavities of non-axisymmetric shape made of bulk ultra-high purity Nb. Since the cavities are produced by complex metal sheet forming processes, followed by a heat treatment (HT) for H outgassing (650 °C, 24 h), there is uncertainty on their mechanical properties after manufacturing and in service conditions (2 K). Mechanical tests at room temperature have been conducted on RRR300 pure Nb samples. The samples were previously submitted, by cold cross-rolling, to different levels of plastic deformation representative of the effective plastic strain seen by the Nb sheets during forming operations. Moreover, a comparison of the mechanical properties of cold cross-rolled samples before and after HT has been established. Results of evolution of the microstructure and hardness are also presented. This study can be of interest for Nb cavities to be submitted to HT at 650 °C, and may help to push the design of novel SRF cavities.

## INTRODUCTION

The Crab Cavities (CC) for HL-LHC project, which operate at 2 K, are highly non-axisymmetric 400 MHz SRF cavities made of ultra-high purity superconducting grade niobium. Their aim is to produce a transverse kick to crossing proton bunches which results in a transverse displacement at the interaction point of the head and the tail of each of the bunches, so as to provide head-on collisions [1][2]. In order to increase the CC quality factor ( $Q_0$ -value) during operation, they are submitted to a thermal treatment for outgassing the hydrogen absorbed, presumably, during the manufacturing and surface cleaning processes [3]. The cavities operate at ultra-high vacuum and are immersed in liquid helium. Thus, the cavities are considered as pressure vessel equipment and shall be structurally assessed according to the corresponding standards to withstand a service pressure of 2.1 bar.

It is known that the recrystallization temperature of pure Nb is around 800°C to 1200°C, this range being highly de-

pendent on the purity, amount of cold work, and prior thermomechanical history of the material. Generally, higher material purity and increased cold work will promote lower recrystallization temperatures [4]. Most of the suppliers perform the annealing of Nb, during the last stages of the manufacturing process, at temperatures around 800°C for typically one or two hours.

Given that the main components of the HL-LHC CC are plastically deformed due to deep drawing operations and that the niobium employed for their manufacturing is of ultra-high purity, a comprehensive study in order to clarify the impact of the heat treatment at 650°C on the mechanical properties has been performed.

In some accelerators employing SRF cavities made of pure Nb submitted to a heat treatment at 800 °C, the material properties used for the structural assessment correspond typically to the properties of a fully annealed RRR300 niobium; in this case the yield strength is around 40 MPa [5]. In order to perform an accurate mechanical assessment of the CC, particularly in the most critical scenario (i.e. when there is the maximum differential pressure at room temperature) the mechanical properties of the cavities following the final heat treatment are of interest.

The aim of the present study is to evaluate the mechanical properties of RRR300 Nb submitted to different levels of cold work after a heat treatment (HT) at 650°C during 24 hours.

## EXPERIMENTAL PROCEDURE

One Nb sheet of 4 mm nominal thickness supplied by Ningxia Orient Tantalum Industry Co. Ltd, (OTIC) and used for the HL-LHC Double Quarter Wave (DQW) Crab Cavity pre-series, was employed. The measured RRR (defined as  $R(300\text{ K})/R(4.2\text{ K})$ ) for the studied sheet is  $\sim 310$ . The chemical composition reported into the material certificate is presented in Table 1.

Table 1: Chemical analysis of a RRR300 Nb sheet belonging to the same ingot, batch, and heat number than the tested sheet (in ppm weight).

Ta	Zr	Fe	Si	W	Ni	Mo
300	5	5	10	<5	<5	<5
Hf	Ti	Cr +Co	H	N	O	C
10	<5	<10	1	8	7	10

\* Research supported by the HL-LHC project.

<sup>†</sup> adria.gallifa@cern.ch

In the as-received condition, the sheets feature a fully annealed microstructure and an average ASTM E112 [6] grain size number of 6 (~45 μm average diameter). Based on the information available, the sheets have undergone a light levelling operation after the last annealing treatment.

A portion of one sheet was sectioned by water jet cutting to obtain ten smaller sheets (hereafter referred as sub-sheets) of 120mm x 120 mm x 4 mm. The sectioned sub-sheets were cross-rolled in two orthogonal directions, corresponding to the rolling and transverse directions of the initial sheet, in order to keep the highest isotropy possible. The rolling process was performed at University of Miskolc (HU) with a Von Roll rolling mill of 1 MN nominal maximum force, employing two high rolling mode at room temperature (RT), in consecutive passes of 5 % thickness reduction and by changing 90° the feeding direction at every pass. The roll diameter and its width are 220 mm. Prior to each pass, the rolls were lubricated with a mineral oil based lubricant through nozzles. The rolling speed was kept constant at 30 m/min throughout the entire rolling process and the force and the torque were recorded for each pass.

The aim was to achieve, by cross-rolling, different levels of cold work representative of the distribution of cold work imposed to the different sub-components of the bare cavity during the deep drawing operations. For this purpose, the approach adopted in the present work employs the effective plastic strain [7], which corresponds to the incrementally cumulated equivalent Von Mises strain during an entire plastic deformation process. This takes into account the triaxiality of the plastic deformation, being typically used to assess the deformation state in highly strained components. In Eq.1,  $\epsilon_{VM}$  is the instantaneous equivalent Von Mises strain [8],  $\epsilon_i$  are the principal components of the strain tensor and  $\nu'$  is the effective Poisson's ratio, which was assumed 0.5 for plastic strains.

$$\epsilon_{VM} = \frac{1}{1 + \nu'} \left[ \frac{1}{2} [(\epsilon_1 - \epsilon_2)^2 + (\epsilon_2 - \epsilon_3)^2 + (\epsilon_3 - \epsilon_1)^2] \right]^{\frac{1}{2}} \quad (1)$$

In Fig. 1, an example of a FE (Finite Element) simulation showing the effective plastic strain induced into one of the sub-components of the Radio Frequency Dipole (RFD) cavity, called the Pole, by the deep drawing process is shown.

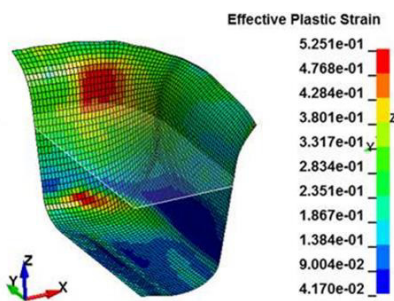


Figure 1: Example of a FE simulation showing the distribution of the effective plastic strain in the RFD CC Pole sub-component due to deep drawing. More information on the simulation and numerical model used can be found in [9].

In Fig. 2, a histogram correlates the surface percentage of the RFD Pole that has been submitted to certain level of effective plastic strain due to the forming operations. The Pole is one of the most strained sub-components during forming and is placed in a structurally critical area of the cavity, thus it is naturally an object of study interest.

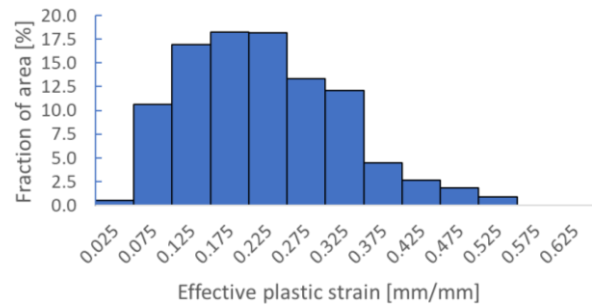


Figure 2: Histogram of the percentage of the RFD Pole surface having seen certain level of effective plastic strain.

In Fig. 3, a plot relating the equivalent Von Mises strain obtained analytically in function of the thickness reduction achieved via cross-rolling is shown, together with the thickness reduction levels selected for the present study (target values).

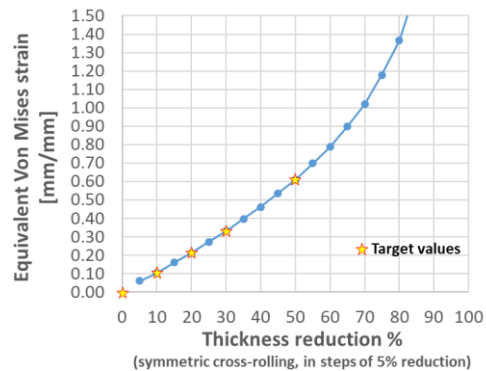


Figure 3: Analytical relationship between thickness reduction by cross-rolling and corresponding equivalent Von Mises strain. The equivalent Von Mises strain values (y-axis) are assumed to be equal to the effective plastic strain, as the principal components of strain are increased monotonically during the rolling process.

The thickness reductions chosen were: 0 % as a reference of non-deformed material, 10 %, 20 % and 30 % in order to induce some of the most frequent effective plastic strain values within the cavity sub-components (according to FE simulations), and 50 % as an extreme value (see Fig. 4).

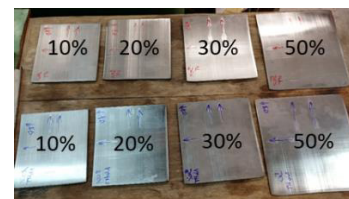


Figure 4: Eight sub-sheets cross-rolled to 10 %, 20 %, 30 % and 50 % nominal thickness reduction respectively. The sheets from the top were eventually submitted to the HT at 650°C for 24h.

Content from this work may be used under the terms of the CC BY 3.0 licence (© 2019). Any distribution of this work must maintain attribution to the author(s), title of the work, publisher, and DOI.

The final thickness achieved and corresponding effective plastic strain are shown in Fig. 5.

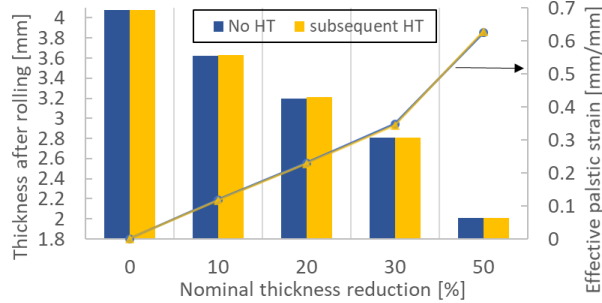


Figure 5: Final thickness for sub-sheets after cross-rolling. In blue sheets that were not heat treated (no HT), in yellow sheets that were heat treated after rolling (subsequent HT).

All the sub-sheets (even those that were not heat treated) were submitted to a Buffered Chemical Polishing (BCP) of 20  $\mu\text{m}$  per side in order to remove potential surface contaminants embedded during the rolling steps.

Five sub-sheets, corresponding to 0, 10, 20, 30, and 50 % nominal thickness reduction, were submitted to the hydrogen degassing heat treatment seen by the bare Crab Cavities prior to its assembly with the rest of the cryomodule. The other five sub-sheets (0, 10, 20, 30, and 50% of thickness reduction) were kept aside, without any heat treatment, for comparison. The HT consists in the following steps: pumping down the furnace below  $5 \cdot 10^{-6}$  mbar pressure, heating at a rate of 200  $^{\circ}\text{C}/\text{h}$  up to 650  $^{\circ}\text{C}$ , soaking at 650  $^{\circ}\text{C}$  during 24 hours and cooling down at a rate of about 50  $^{\circ}\text{C}/\text{h}$ . The pressure at the end of the treatment is in the low  $10^{-7}$  mbar range. The furnace is vented by  $\text{N}_2$  gas only when the temperature of the cavity is below 100  $^{\circ}\text{C}$ .

Three tensile specimens for every sub-sheet, thus a total of 30 specimens (15 no HT and 15 HT), were cut by Electrical Discharge Machining (EDM) cutting technique. The longitudinal axis of the specimens was aligned with the rolling direction of the initial sheet.

The geometry of the tensile specimens (Fig. 6) was adapted from ISO 6892-4 [10], in order to be able to use the same specimen geometry and tooling equipment for tests at RT and for tests at cryogenic temperature\*.

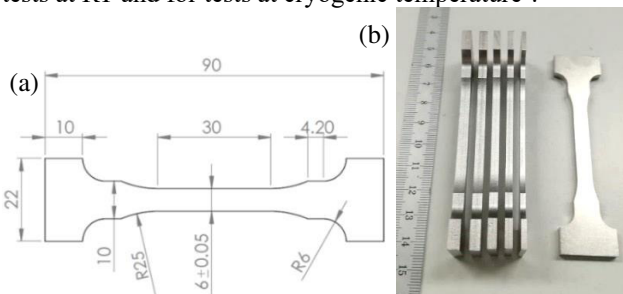


Figure 6: a) Tensile specimen drawing. b) Ready-to-test specimens of different thickness, from left to right: 0, 10, 20, 30 and 50 % thickness reductions.

\* Tensile tests at 4 K are foreseen in the scope of this study but not presented in the present conference paper.

A FE simulation confirmed that the modified design did not enhance any unexpected stress concentration.

After EDM cutting, all specimens were submitted to a BCP of 30  $\mu\text{m}$  per side, to remove the surface oxidation and potential micro cracks introduced by the above mentioned sectioning technique.

All the tensile tests, done at room temperature, were conducted at a fixed displacement rate of 0.17 mm/min, corresponding to a strain rate of 0.0068 mm/mm/min, just below the maximum deformation rate imposed in the ASTM B393 [11] to track the yield point. The strain rate was controlled by a mechanical extensometer of  $L_0=25$  mm. A pre-load in the order of 50 N was applied prior to each test.

The microstructure of the cross-rolled sheets before and after heat treatment was observed. The samples were sectioned with an abrasive cutting machine, were ground with SiC grinding paper up to P2400 and polished with colloidal silica of 0.05  $\mu\text{m}$  particle size. A chemical etching employing a mixture of commercial  $\text{HNO}_3$ ,  $\text{HCl}$  and  $\text{HF}$  acids in the ratio 3:2:1 was used. HV0.1 hardness profiles across the thickness were performed to all the sheets before and after HT.

## RESULTS AND DISCUSSION

Figure 7 shows the engineering stress-strain curves for specimens cross-rolled to the different thickness reductions, before and after HT respectively.

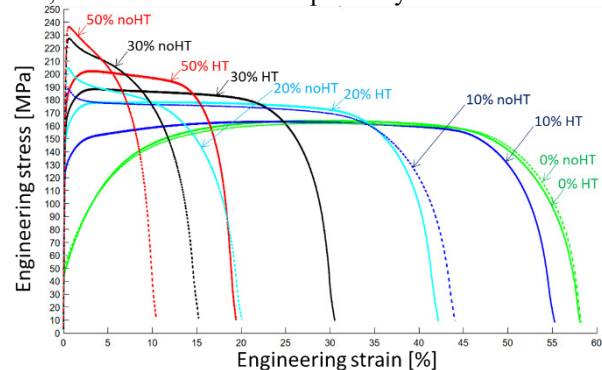


Figure 7: Engineering stress-strain curves at RT. Only one representative sample for each thickness reduction before and after HT is shown for easier reading. Same colour denotes same thickness reduction.

Each of the specimens after cross-rolling, features very similar yield strength ( $R_{p0.2}$ ) and tensile strength ( $R_m$ ) values, denoting a reduced strain hardening. Therefore, after reaching  $R_m$ , the specimens will promptly develop a non-homogeneous and localized plastic deformation (i.e. necking). This effect is more present for higher thickness reductions. After heat treatment, on the contrary, the strain hardening phenomenon is recovered to a certain extent, so that after reaching  $R_m$ , there is a “plateau” at stresses close to the ultimate strength and the necking starts to form at higher strains.

In Fig. 8 and Fig. 9, an overview of the evolution of the yield strength ( $R_{p0.2}$ ), the ultimate strength ( $R_m$ ) and the elongation at break ( $A_{25mm}$ ) before and after HT are presented. Both graphs have been plotted using data from a total of 28 specimens (13 before HT and 15 after HT).

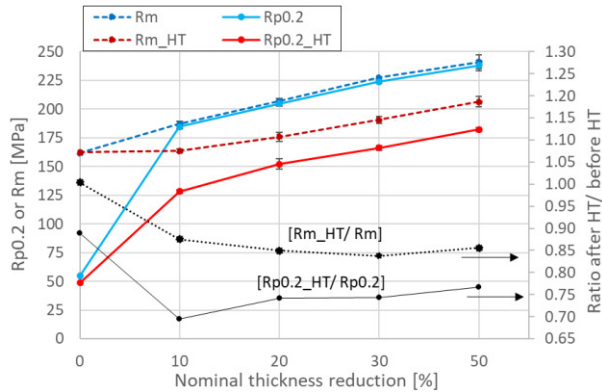


Figure 8: Overview of the  $R_m$  and  $R_{p0.2}$  values before and after HT vs. thickness reduction by cross-rolling. Error bars represent one standard deviation (note that deviations are very low, indicating high repeatability). Secondary axis indicates the ratio (after HT/before HT).

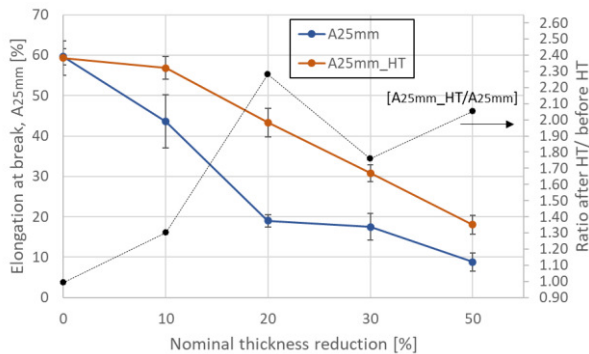


Figure 9: Overview of the  $A_{25mm}$  values before and after HT in function of the thickness reduction achieved by cross-rolling. Error bars represent one standard deviation. Secondary axis indicates the ratio (after HT/before HT).

There is no full recrystallization after the heat treatment, for none of the levels of plastic deformation. However, a recovery annealing (i.e. partial annealing) has taken place, probably due to a relief of strain energy by a rearrangement of the dislocations introduced by cold work. During the recovery, dislocation density decreases, and dislocations assume low-energy configurations [12][13]. Note that the drop in  $R_{p0.2}$  after HT is more important than the drop in  $R_m$  for all thickness reductions (see Fig. 8). The decrease in  $R_{p0.2}$  is practically constant, of about 50 MPa, for the four applied thickness reductions. Therefore, one can guess that due to the HT, there is a fixed reduction of the energy needed to yield. This is probably associated to a fixed reduction of dislocation density, which might be limited by the atomic diffusion at 650 °C. For the as-received sheet, the  $R_m$  and elongation at break remain constant after HT, but the  $R_{p0.2}$  is reduced by a 10 %. Although not visible in the figures shown, the initial part of the stress-strain curve

for the as-received sheet after HT features an upper and lower yield strength. For 10% thickness reduction, HT brings back the tensile strength to the value of the as-received sample. It has to be noted (see Fig. 9) that, even for the highest deformed specimens (50 % thickness reduction) the elongation at break is still around 10 % after cross rolling, being recovered up to almost 20% after HT.

After the HT at 650 °C for 24h, the decrease in mechanical properties ( $R_{p0.2}$  and  $R_m$ ) is lower than the increase introduced formerly by cold cross-rolling. During cold cross-rolling, two strengthening effects take place to confer the material its final mechanical properties: on one hand the change in the grain boundaries distribution due to the change in the grain aspect ratio (see Fig. 10) and presumably the creation of micro grains (this is related to the Hall-Petch effect) and on the other the creation of new dislocations, thus an increased dislocation density.

As shown in Fig. 10, since the microstructural grain shape and size appear to be unchanged after HT, it may be deduced that the HT has a more important impact mainly in the second effect, by decreasing the dislocation density.

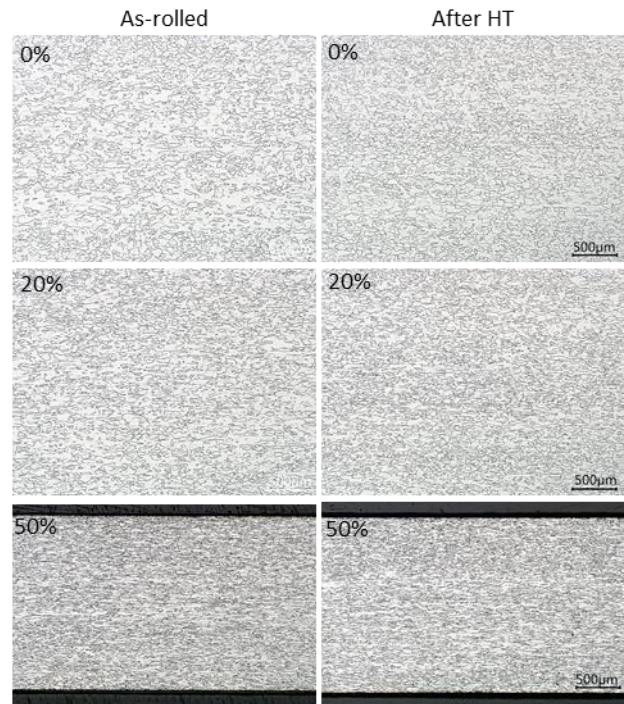


Figure 10: Microstructure in the plane formed by the short transverse and rolling directions for as received sheet (0%) and 20% and 50% thickness reductions, before and after HT. Original magnification 100x.

Therefore, after HT there is certain loss in mechanical properties ( $R_m$  and  $R_{p0.2}$ ) and also an increase in elongation at break: the Hall-Petch effect is still present but the dislocation density has presumably decreased.

In Fig. 11 it can be seen that after HT there is generally a decrease in hardness, except for the as-received sheet; also it has to be noted that fluctuation of HV0.1 hardness values is growing for larger thickness reductions, as expected.

Content from this work may be used under the terms of the CC BY 3.0 licence (© 2019). Any distribution of this work must maintain attribution to the author(s), title of the work, publisher, and DOI.

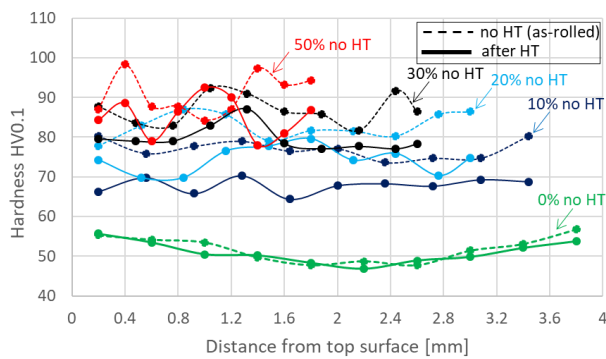


Figure 11: HV0.1 hardness profiles across the thickness of all the specimens, before and after HT respectively.

For the as-received material (levelled product) hardness is higher close to the surface due to the bending and counter-bending cycles that take place during levelling operation, and lower at the mid-thickness, which corresponds to the neutral fibre. This characteristic profile remains unchanged after HT.

Given that the HT does not produce a full recrystallization, it is assumed that it would be beneficial for the structural integrity of the cavity to harden the different sub-components via cold work, as done during forming operations. However, the impact of having higher dislocation densities (with respect to fully annealed Nb) on the RF performance would need to be checked. The fact of not reaching the maximum RF performance during operation may be related to some extent to the fact that dislocations created during cold working operations and also grain boundary distortions are still present in the Nb crystalline structure after HT. Further investigations relating RF performance with for instance, dislocation density, would be needed to confirm this point.

According to FE simulations (as shown in Fig. 1 and Fig. 2), the main surface of the RFD pole (and the bare cavity) is plastically deformed during deep drawing operations, thus, its mechanical properties are expected to be significantly higher than the properties of the as-received material. If the approach used in this paper (effective plastic strain) is proven to be valid to correlate cross-rolling and deep drawing operations, the mechanical properties of the cavity even after HT, would also be higher than the ones of the as-received material, thus enhancing the cavities structural integrity (see Fig. 12).

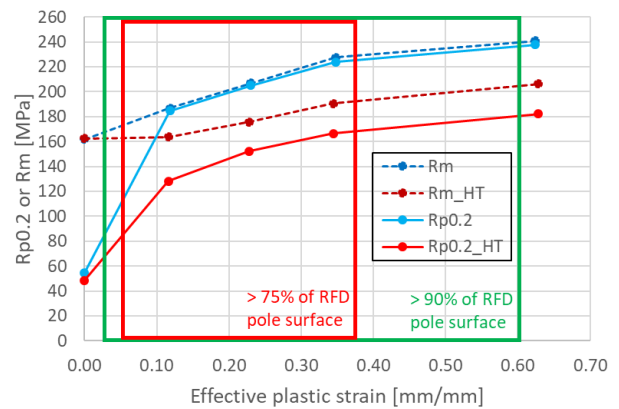


Figure 12:  $Rp_{0.2}$  and  $R_m$  vs. effective plastic strain, before and after HT. Rectangle boxes contain the range of effective plastic strains in 75 and 90% of RFD pole surface respectively. The graph is similar to Fig. 8, but x-axis has been replaced by effective plastic strain.

## CONCLUSION

A 4 mm thickness Nb sheet was cold cross-rolled in order to achieve different thickness reductions representative of the effective plastic strain that the Nb sheets experience during the forming operations of the CC sub-components. The evolution of the mechanical properties at room temperature (including  $Rp_{0.2}$ ,  $R_m$ , elongation at break and hardness) and of the microstructure were presented, for the cross-rolled specimens before and after a hydrogen degassing heat treatment at 650 °C for 24 h.

It has been proven that there is no full recrystallization after heat treatment, for none of the levels of plastic deformation induced by cold cross-rolling. However, it is clear that certain recovery annealing has occurred (which is stronger for cross-rolled material and marginal for as-received material). After cross-rolling and HT, the specimens showed higher mechanical properties than the as-received material. Therefore, as a preliminary conclusion it can be stated that some of the parts of the Crab Cavities with lower mechanical properties ( $Rp_{0.2}$  and  $R_m$ ) would be the ones non-plastically deformed during the manufacturing process (i.e. parts only machined and also the lowest deformed regions during deep drawing). Caution has to be taken when relating the results from this study to the behaviour of the real cavity, since the introduction of cold work (i.e. the creation and evolution of dislocation motion and interaction) via cross-rolling and deep drawing may differ. Further studies, including investigation on real cavity samples and tensile tests at 4 K, are foreseen in order to clarify this relationship and to complement the present study.

## ACKNOWLEDGEMENTS

The authors would like to thank S. Forel for performing the BCP, A. Mongelluzzo for the heat treatment and S. Calatroni and S. Sgobba for the useful discussions.

## REFERENCES

- [1] R. Calaga, "CRAB cavities for the LHC upgrade". No. CERN--2012-006. 2012.

- [2] “High-Luminosity Large Hadron Collider (HL-LHC). Preliminary Design Report”, edited by G. Apollinari, I. Béjar Alonso, O. Brüning, M. Lamont, L. Rossi, CERN-2015-005 (CERN, Geneva, 2015), DOI: <http://dx.doi.org/10.5170/CERN-2015-005>
- [3] M. Hakovirta, “Measurements of hydrogen content in bulk niobium by thermal desorption spectroscopy”. No. CERN-EST-2002-005-SM. 2002.
- [4] ASM Handbook. “Volume 4, Heat Treating”. Materials Park, OH :ASM International, 1991.
- [5] T.J. Peterson, et al. "Pure niobium as a pressure vessel material." *AIP Conference Proceedings*, Vol. 1218, No. 1, pp. 839-848 AIP, 2010.
- [6] ASTM E112-13, Standard Test Methods for Determining Average Grain Size, ASTM International, West Conshohocken, PA, 2013.
- [7] J.O. Hallquist, "LS-DYNA theory manual", Livermore software Technology corporation, 2006.
- [8] [https://www.sharcnet.ca/Software/Ansys/16.2.3/engus/help/wb\\_sim/ds\\_Equiv\\_Stress.html](https://www.sharcnet.ca/Software/Ansys/16.2.3/engus/help/wb_sim/ds_Equiv_Stress.html)
- [9] A. Amorim Carvalho et al., “Advanced Design of Tooling for Sheet-Metal Forming through Numerical Simulations in the Scope of SRF Crab cavities at CERN”, *ESAFORM 2019 proceedings*, 2019.
- [10] ISO 6892-4:2015, “Metallic materials -- Tensile testing -- Part 4: Method of test in liquid helium”
- [11] ASTM B393-18, Standard Specification for Niobium and Niobium Alloy Strip, Sheet, and Plate, ASTM International, West Conshohocken, PA, 2018.
- [12] W.D. Callister, D. William, D.G. Rethwisch. “Materials science and engineering: an introduction”, Vol. 7, New York: John Wiley & Sons, 2007.
- [13] F. J. Humphreys, M. Hatherly, “Recrystallization and related annealing phenomena”, Elsevier, 2012.